Biomedical Signal Processing and Control 8 (2013) 830–837

Contents lists available at ScienceDirect

Biomedical Signal Processing and Control

journal homepage: www.elsevier.com/locate/bspc

Analysis of parametric estimation of head tissue conductivities using Electrical Impedance Tomography

Mariano Fernández-Corazza[a,b,*], Leandro Beltrachini[a,b], Nicolás von Ellenrieder[a,b], Carlos H. Muravchik[a,c]

[a] Laboratorio de Electrónica Industrial, Control e Instrumentación (LEICI), Departamento de Electrotecnia, Facultad de Ingeniería, Universidad Nacional de La Plata, Calle 48 y 116, CC91 (1900), La Plata, Buenos Aires, Argentina
[b] Consejo Nacional de Investigaciones Científicas y Técnicas (CONICET), Argentina
[c] Comisión de Investigaciones Científicas de la Provincia de Buenos Aires (CICpBA), Argentina

ARTICLE INFO

Article history:
Received 6 February 2013
Received in revised form 24 June 2013
Accepted 5 August 2013

Keywords:
Electrical Impedance Tomography
Cramér-Rao Bound
Maximum Likelihood Estimator
Electrical conductivity estimation
Skull anisotropy
Finite Element Method

ABSTRACT

We study the theoretical performance of using Electrical Impedance Tomography (EIT) to measure the conductivity of the main tissues of the head. The governing equations are solved using the Finite Element Method for realistically shaped head models with isotropic and anisotropic electrical conductivities. We focus on the Electroencephalography (EEG) signal frequency range since EEG source localization is the assumed application. We obtain the Cramér-Rao Lower Bound (CRLB) to find the minimum conductivity estimation error expected with EIT measurements. The more convenient electrode pairs selected for current injection from a typical EEG array are determined from the CRLB. Moreover, using simulated data, the Maximum Likelihood Estimator of the conductivity parameters is shown to be close to the CRLB for a relatively low number of measurements. The results support the idea of using EIT as a low-cost and practical tool for individually measure the conductivity of the head tissues, and to use them when solving the EEG source localization. Even when the conductivity of the soft tissues of the head is available from Diffusion Tensor Imaging, EIT can complement the electrical model with the estimation of the skull and scalp conductivities.

1. Introduction

Electric models of the human head, as used in Electroencephalography (EEG) source localization, require an electrical conductivity map of the head. Usually, this map is built as a layered model, with each layer representing a different tissue. The shape of the layers is either assumed spherical, ellipsoidal, or obtained by segmenting Magnetic Resonance (MR) images. Then, the electrical conductivity values for each tissue are usually selected from existing studies [1–5]. However, there is a large variation in the values found in the literature, depending on the measurement method, and probably due to inter-subject variability [6]. The use of incorrect values in the head model could lead to erroneous solutions of the neural source estimation [7–9]. A possible solution to this problem is the use of Electrical Impedance Tomography (EIT) measurements from the subject under study to estimate the conductivity of the main tissues of the head. As EIT is portable and relatively cheap, this is an advantage over other methods such as MR (particularly, Diffusion Tensor Imaging (DTI)) or Computed Tomography (CT) that could be used with the same purpose. Also, EIT can estimate the skull conductivity, which cannot be obtained from DTI. Most of the skull conductivity values found in the above mentioned literature are based on *in vitro* or *in vivo* measurements with a four electrode system. In EIT, the same electrodes and acquisition system of EEG could be used in combination with an electric current source to estimate *in vivo* the tissue conductivities.

Electrical Impedance Tomography (EIT) on the head consists of injecting electrical currents on known points on the scalp and measuring the resulting electric potential distribution on the scalp to infer the electrical impedance map of the whole head volume. An inconvenience with EIT impedance mapping is that even when using an array with a large number of electrodes, the spatial resolution of the resulting map is quite low [10]. To overcome this, it is possible to combine the high spatial resolution of the MR segmentation in tissues, with the EIT technique to estimate the electrical

* Corresponding author at: Laboratorio de Electrónica Industrial, Control e Instrumentación (LEICI), Departamento de Electrotecnia, Facultad de Ingeniería, Universidad Nacional de La Plata, Calle 48 y 116, CC91 (1900), La Plata, Buenos Aires, Argentina. Tel.: +54 2214259306; fax: +54 2214259306.
E-mail addresses: marianof.corazza@ing.unlp.edu.ar, marianofco@gmail.com (M. Fernández-Corazza), lbeltra@ing.unlp.edu.ar (L. Beltrachini), nellen@ieee.org (N. von Ellenrieder), carlosm@ing.unlp.edu.ar (C.H. Muravchik).

1746-8094/$ – see front matter © 2013 Elsevier Ltd. All rights reserved.
http://dx.doi.org/10.1016/j.bspc.2013.08.003

conductivity of each layer [11,12]. In this way, parametric estimation tools are used to solve the EIT inverse problem (EIT IP), i.e. the construction of the conductivity map.

The skull is highly resistive compared to the surrounding tissues, acting as an electrical shield between the scalp and the brain. It is mostly composed by a sandwich of two layers of compact bone with a layer of spongy bone in the middle [4]. Several models have been proposed for the skull adopting isotropic conductivities to each type of bone [13], a single homogeneous isotropic conductivity, localized but isotropic conductivities [14], or homogeneous but anisotropic models [9,13], where the tangential conductivity is higher than the radial (or transversal) one. The relevance of considering the skull anisotropy has also been analyzed [9]. Several studies measured the skull conductivity and its anisotropy ratio [1,2,15,16]. Existing reports show skull conductivity values ranging from 0.04 S/m to 0.004 S/m [1,2,4,16] (and even some values outside this range have been discussed). The radial:tangential anisotropy ratio was initially supposed to be 1:10 [1], but recent studies suggest that it is lower, ranging from 1:1.6 to 1:6 [3,9] considering the 1:10 ratio as an upper limit. Our hypothesis is that the ratio is still uncertain and a wide range of anisotropic conductivity ratios (from 1:1 to 1:10) is evaluated.

The scalp is the first compartment that the current passes through, playing a major role in EIT [4]. It can also be modeled as inhomogeneous because it has zones with muscles, fat and different skin thickness. Homogeneous but anisotropic models with transversal to tangential ratio of 1:1.5 have been also used [8]. As the conductivity of this tissue is higher than the skull's, its relative inhomogeneities are usually neglected and a single isotropic conductivity is assigned to this layer. This value is also uncertain since only few studies have been performed to measure it [4]. So, EIT can also be applied to obtain a scalp conductivity estimate.

The innermost cavity is the most complex as it includes cerebrospinal fluid (CSF), gray matter, and white matter. Assigning to it a single conductivity value is nowadays an oversimplification of the problem and recent studies also highlight the relevance of considering anisotropy within the white matter [8,9,17]. The diffusion of water over the tissues (MR-DTI) can be used to build an anisotropic conductivity map of the CSF, white and gray matter, by means of a linear transform of each tensor eigenvalue [18]. Averaged conductivity distributions can be used if the patient specific resonance is not available [19].

We assess the performance of using EIT to estimate the conductivity values of the scalp, skull, and brain. For the first two tissues we analyze homogeneous isotropic and anisotropic conductivities, whereas for the brain, we assign a unique isotopic value or a realistic inhomogeneous and anisotropic map based on a DTI atlas. We use this to analyze the influence of the *a priori* knowledge of the tensorial map of the brain conductivity (that could be obtained from DTI) in the EIT parametric estimation. The Cramér-Rao Lower Bound (CRLB) is computed for the unknown parameters, allowing us to quantify the performance of the method independently of the specific algorithm used to estimate the conductivity values, and to detect convenient electrode pairs for the current injection. This builds upon our preliminary study [20], where we analyzed convenient pairs using a simple spherical head model with a particular estimation algorithm. In contrast to other studies [11,12], in this work we use detailed realistic head models including the estimation of the anisotropic components of the tissue conductivities. To the best of our knowledge, our parametric EIT estimation analysis introduces accounting for anisotropic components of the scalp and skull conductivity tensors. Finally, we compute the Maximum Likelihood Estimator (MLE) to solve the EIT IP using simulated signals with additive noise and we show that its performance is close to the bound even for a limited number of measurements.

2. Methods

2.1. Forward problem solution

The EIT forward problem (FP) consists in calculating the electric potential distribution on the scalp as a result of current injection, assuming that the electrical conductivities are known. In the EEG frequency range, this is a quasistatic problem with Neumann boundary conditions [21]. The governing equations are

$$\begin{cases} \vec{\nabla}\cdot\left(\boldsymbol{\sigma}\left(\vec{x}\right)\vec{\nabla}\boldsymbol{\Phi}\left(\vec{x}\right)\right)=0, & \text{in}\,\Omega \\ \boldsymbol{\sigma}\left(\vec{x}\right)\left(\vec{\nabla}\boldsymbol{\Phi}\left(\vec{x}\right)\right)\cdot\hat{n}=j(\vec{x}), & \text{in}\,\delta\Omega \end{cases} \tag{1}$$

where $\vec{x}=(x,y,z)$ represents a generic point in the head, $\boldsymbol{\Phi}$ is the electric potential, $\boldsymbol{\sigma}$ represents the conductivity tensor, Ω is the head volume and $\delta\Omega$ is its outer surface, $\hat{n}$ is the normal unit vector, and j is the normal component of the current density on the boundary.

The FP can be solved analytically for spherical geometries and isotropic conductivities [20,22]. When using arbitrary shapes, numerical methods such as the Boundary Element Method (BEM) or the Finite Element Method (FEM) are required to solve the problem. We use the FEM because it admits the anisotropy of the tissues. Existing studies have validated the use of FEM for EIT purposes [23].

Using linear basis functions in the FEM with tetrahedral elements (and n nodes), the problem is converted into a linear system of equations with the form $KU=F$ (see Appendix A) where K is the $n\times n$ *stiffness matrix* that includes information of the head geometry and conductivity, U is the unknown $n\times 1$ vector of the potential at the n nodes of the volume tessellation, and F is the $n\times 1$ independent vector that includes the information of the electric current.

For simplicity, the electrodes are assumed to be a point with no surface as the electrode area is much smaller than the total area of the external head surface [24]. Complete electrode models could also be considered as in [8].

2.2. Signal model

Based on the FP we may write a sample Y of the signal at the electrodes as

$$\mathbf{Y}=MU+W=MK^{-1}F+W, \tag{2}$$

where M is an $m\times n$ sparse selection matrix that selects the elements of U corresponding to the nodes located at the position of the m measurement electrodes, and W is a noise term. The noise in the measurements should contemplate two sources; the noise of the amplifiers and the skin-electrode contact impedance, and the electrical activity of the brain, which is an undesired noise term in this EIT application. The latter may have larger amplitude and could lead to a large variance of the estimated parameters [20]. However, as it is spatially and temporally correlated, an appropriate selection of the current waveform and data processing mitigates its effect if a sufficient number of temporal samples are available [29].

2.3. Head models

The head models adopted for this study have a realistic shape and are composed by three layers representing brain, skull, and scalp. In order to obtain general results, average models are chosen for the head shape and the surfaces that delimit the layers. They are obtained from the ICBM152 atlas [27], which is an average of 152 healthy subjects. We analyze three models:

Isotropic: The three layers are considered homogeneous and isotropic with their three parameters of interest; the electrical conductivities of each layer (σ_{sc}, σ_{sk}, σ_{br}).

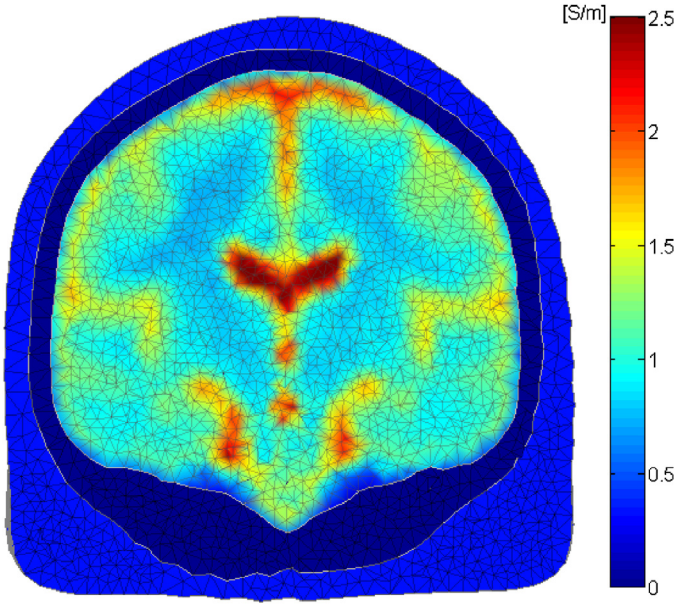

Fig. 1. Geometry of the head model with its subdivision in three layers (coronal slice). The discretization into tetrahedrons is also shown. For the innermost layer, the color scale depicts the conductivity map derived from the DTI atlas and used in the *Partially Isotropic* and the *Anisotropic* head models. (For interpretation of the references to color in this figure legend, the reader is referred to the web version of the article.)

Partially Isotropic: The scalp and skull layers are identical to the previous model, but in this case the conductivity map of the inner cavity (σ_{br}^{dti}) is obtained from the ICBM-DTI-81 atlas [19]. Fig. 1 shows the mean conductivity map used in this model. The aim with this model is to quantify the improvement in the estimation of the skull and scalp conductivities when the conductivity map of the brain is known.

Anisotropic: The scalp and skull conductivities are split in two parameters that allow us to model the anisotropy of these tissues. The brain conductivity is the same as in the previous model, i.e. it is obtained based on DTI. There are four parameters of interest: tangential scalp conductivity (σ_{sc}^{t}), radial scalp conductivity (σ_{sc}^{r}), tangential skull conductivity (σ_{sk}^{t}), and radial skull conductivity (σ_{sk}^{r}).

For each model, the resultant FEM expressions are the following (details are shown in Appendix A):

$$K(\boldsymbol{\theta})U = (\sigma_{sc}K_{sc} + \sigma_{sk}K_{sk} + \sigma_{br}K_{br})U = F, \tag{3}$$

for the *Isotropic* model,

$$K(\boldsymbol{\theta})U = (\sigma_{sc}K_{sc} + \sigma_{sk}K_{sk} + K_{br}^{dti})U = F, \tag{4}$$

for the *Partially Isotropic* model, and

$$K(\boldsymbol{\theta})U = (\sigma_{sk}^{t}K_{sk}^{t} + \sigma_{sk}^{r}K_{sk}^{r} + \sigma_{sc}^{t}K_{sc}^{t} + \sigma_{sc}^{r}K_{sc}^{r} + K_{br}^{dti})U = F, \tag{5}$$

for the *Anisotropic* model, where $\boldsymbol{\theta}$ is the vector of unknown parameters σ_i, and K_l, K_l^t and K_l^r are the $n \times n$ *stiffness matrices* for each region l (*sk* for skull, *sc* for scalp and *br* for brain). For the last two models, the *stiffness matrix* of the brain K_{br}^{dti} was obtained from DTI based on a linear transformation of the largest eigenvalues [18].

2.4. Cramér-Rao Lower Bound and Maximum Likelihood Estimator

The CRLB is useful to quantify the theoretical performance of parameter estimation, providing a lower bound on the error variance of any unbiased estimator. In the three head models, we use it to assess the quality of EIT estimates of the parameters. Then, if $\hat{\boldsymbol{\theta}}$ is an unbiased estimator of $\boldsymbol{\theta}$,

$$Cov\{\hat{\boldsymbol{\theta}}\} \geq CRLB(\boldsymbol{\theta}) = J^{-1}(\boldsymbol{\theta}), \tag{6}$$

where the matrix inequality implies that the difference is positive semidefinite, J is the Fisher information matrix, and *Cov* stands for covariance. For signals in White Gaussian Noise such as (2), J is given by

$$[J(\boldsymbol{\theta})]_{ij} = \frac{S}{\sigma_w^2}\left(\frac{\partial \boldsymbol{\mu}(\boldsymbol{\theta})}{\partial \theta_i}\right)^T \left(\frac{\partial \boldsymbol{\mu}(\boldsymbol{\theta})}{\partial \theta_j}\right), \tag{7}$$

where $\boldsymbol{\mu}(\boldsymbol{\theta})$ is the expected value of the signal Y, S is the total number of samples or measurements, and σ_w is the noise standard deviation. [30]. From (2), the expected value is

$$\boldsymbol{\mu}(\boldsymbol{\theta}) = MU = MK(\boldsymbol{\theta})^{-1}F, \tag{8}$$

and its partial derivative is

$$\frac{\partial \boldsymbol{\mu}(\boldsymbol{\theta})}{\partial \theta_i} = M\left(-K^{-1}\frac{\partial K}{\partial \theta_i}K^{-1}\right)F = -MK^{-1}\frac{\partial K}{\partial \theta_i}U. \tag{9}$$

The partial derivatives of K respect to each parameter θ_i can be easily obtained from Eqs. (3), (4) or (5).

For each parameter θ_i, we define the *Coefficient of Variation Bound (CVB)* as

$$CVB_i = \frac{\sqrt{CRLB_{ii}}}{\theta_i}, \tag{10}$$

where θ_i is the reference value for that parameter, and $CRLB_{ii}$ is the ith element of the diagonal of the CRLB matrix. This coefficient is equivalent to a bound on the relative standard deviation of each parameter and we use it to analyze the results.

The EIT IP involves estimating the model parameters (i.e. electrical conductivity values) based on the electric potential measurements from the electrodes. We derive the MLE to solve this problem under a Gaussian measurement model [30]. The MLE for the parameter vector $\boldsymbol{\theta}$ is

$$\boldsymbol{\theta}^{ML} = \min_{\boldsymbol{\theta}}\{(\hat{Y} - MK^{-1}(\boldsymbol{\theta})F)^T(\hat{Y} - MK^{-1}(\boldsymbol{\theta})F)\}, \tag{11}$$

where the $m \times 1$ vector $\hat{Y}$ is the average of the S measurements. Several numerical optimization methods can be used to solve (11). We use the classic Newton's method as the partial derivatives needed for the Gradient and Hessian of (11) can be found as in (9).

To present the results we define the *Estimator Coefficient of Variation (ECV)* for each parameter θ_i as:

$$ECV_i = \frac{\sqrt{Var(\theta_i^{ML})}}{\theta_i}, \tag{12}$$

where *Var* stands for variance.

Since the MLE is an efficient estimator, when the number of measurements S grows, the ECV tends to the CVB. We analyze the behavior of the MLE in a practical situation, for a reasonable value of S.

2.5. CRLB computation and simulations

For the three head models described in Section 2.3 we compute the CVB to study the performance of the method and to infer convenient electrode pairs. We also simulate measurements to test the MLE. In this section we describe and state the adopted values and conditions used to both compute the CVB and simulate the measurements.

Since we propose to perform the EIT data acquisition with the same equipment used for EEG studies, and immediately before or

Table 1
Reference values of conductivity adopted for this study [S/m].

Model	Scalp conductivity		Skull conductivity		Brain conductivity
Isotropic	0.4		0.004–0.04		0.3
Partially Isotropic	0.4		0.004–0.04		DTI
Anisotropic	Tangential	Radial	Tangential	Radial	
	0.45	0.3	0.01–0.014	0.01–0.0014	DTI
(Radial:tangential ratio)	1:1.5		1:1–1:10		

after the EEG data acquisition, we use an electrode placement based on a subset of 64 electrodes of the EEG 10-10 standard system.

We assume the current injection involves one electrode pair while the remaining electrodes measure the resulting electric potential distribution, so that $m = 62$. For its use in human patients, medical equipment must comply with the International Electrotechnical Commission 60601 standard (IEC60601) which specifies a patient auxiliary current limit of 100 μA when the frequency is between 0.1 Hz and 1 kHz [25,26]. Since in this frequency range the quasistatic approximation of Maxwell equations holds, the results are independent of the actual frequency value. We assume that the frequency of the injected current signal is in this range and that the current intensity is 100 μA.

We analyze 16 different pairs for the current injection, a representative subset of the 2016 possible electrode pairs, which cover a range of *a priori* favorable to unfavorable situations. This is based on a preliminary study with a simple spherical head model, where we found that pairs with a large angle between them and a high number of other electrodes surrounding them, were the most favorable configurations [20]. As stated in the Introduction, determining which pairs are better to perform the estimation is one of the main objectives of this work.

To solve the linear problems in Eqs. (2), (8), (9), and in the Hessian matrix computation, we use a biconjugate gradient algorithm that can handle sparse matrices [28]. The tetrahedral mesh used for the three models has a total of 79,725 nodes or vertices (n) and 494,450 elements or tetrahedrons, where 137,072, 42,580 and 314,798 correspond to the scalp, skull, and brain layers respectively (Fig. 1).

In the *Isotropic* and *Partially Isotropic* models, we select the reference scalp and brain conductivity values similar to those frequently found in the literature: $\sigma_{sc} = 0.4$, and $\sigma_{br} = 0.3$ S/m [10]. The poor conductivity of the skull leads to a strong influence of this parameter on the estimates. In view of the extremely wide range of values found for it in the literature [4], we analyze different scenarios varying this parameter from 0.004 to 0.04 S/m.

In the *Anisotropic* model, the radial:tangential conductivity ratio is chosen as 1:1.5 for the scalp, according to an existing study [4]. For the skull there is again a wide range of ratios, so we analyze values ranging from 1:1 (isotropic) to 1:10 (upper limit). In each case, the values are chosen so that the traces of the different conductivity tensors $\boldsymbol{\sigma}(\vec{x})$ are equal to the trace of the isotropic tensor, i.e. $\mathrm{Tr}\{\boldsymbol{\sigma}(\vec{x})\} = 3 \times \sigma_{sc}$ if $\vec{x}$ is a point in the scalp and $\mathrm{Tr}\{\boldsymbol{\sigma}(\vec{x})\} = 3 \times \sigma_{sk}$ if $\vec{x}$ is a point in the skull. The resulting values are $\sigma^t_{sc} = 0.45$ S/m, $\sigma^r_{sc} = 0.3$ S/m, σ^t_{sk} ranging from 0.01 to 0.014 S/m, and σ^r_{sk} ranging from 0.01 to 0.0014 S/m. In Table 1 we summarize the reference values selected for the parameters of the three models.

For the CBV computation, we consider 50 independent time samples S and we assume that this is a quantity large enough to neglect the brain activity noise [29]. Then, $W \sim \mathcal{N}(0, \sigma_w^2 I)$ is independent among channels and among time samples, where I is the identity matrix. We choose a typical noise standard deviation $\sigma_w = 1$ μV that accounts for the electronic noise and for a possible uncorrelated residual term of the brain activity. This value is used in Eq. (7) to compute the CVB and also to generate the Gaussian noise realizations W in the simulated measurements Y of Eq. (2).

For the MLE minimization, the initial values for Newton's method are chosen to be lower than the reference conductivities (uniformly distributed from 50 to 100% of the reference values), and the method is set to stop after the sixth iteration. It was empirically found that the numerical stability and speed of convergence was better for initial values lower than the reference conductivities, and that the method stagnated after six iterations.

For each current injection pair we simulate 20 sets of $S = 50$ measurements with independent noise realizations. The parametric estimation is performed for each set using the MLE formula of Eq. (2), where $\hat{Y}$ is the mean of the 50 measurements. The different sets are used to obtain the variance of the MLE, which is required to obtain the ECV and to compare it to the CVB.

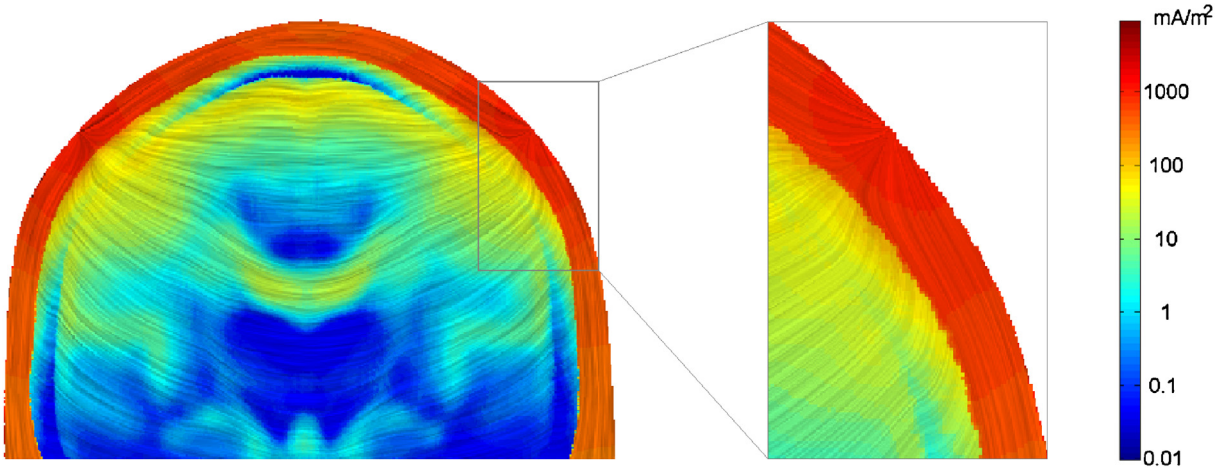

Fig. 2. Current flow on a coronal slice when the C3–C4 is the current injection pair. The gray lines show the current direction and the color scale indicates the amplitude of the current density. (For interpretation of the references to color in this figure legend, the reader is referred to the web version of the article.)

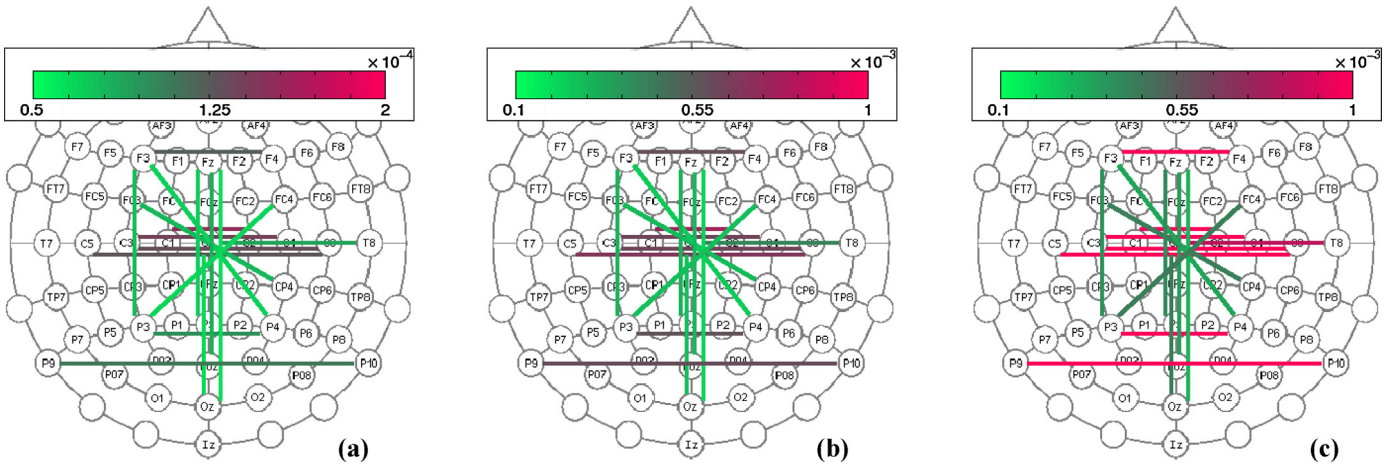

Fig. 3. CVB for the *Isotropic* head model: (a) scalp conductivity, (b) skull conductivity and (c) brain conductivity. The color of each line indicates the CVB value obtained when the current is applied using the electrodes connected by that line. Note that the diagrams have different scales.

3. Results and discussion

We solved the FP as described in the previous section, and as an example, in Fig. 2 we show the current flow in the head when the injection electrodes are C3 and C4. The lines show the current direction and the color scale indicates the amplitude of the current density.

The derivation of the CRLB allows us to obtain several useful results regarding the selection of the electrode pair for current injection. Figs. 3 and 4 show the CVB of selected injection pairs for the three head models with these conductivity values for the skull: $\sigma_{sk} = 0.01\,\mathrm{S/m}$, $\sigma^{t}_{sk} = 0.014\,\mathrm{S/m}$, and $\sigma^{r}_{sk} = 0.0014\,\mathrm{S/m}$. For each parameter, the color of the connection line is proportional to the CVB when the electric current is injected by the two connected

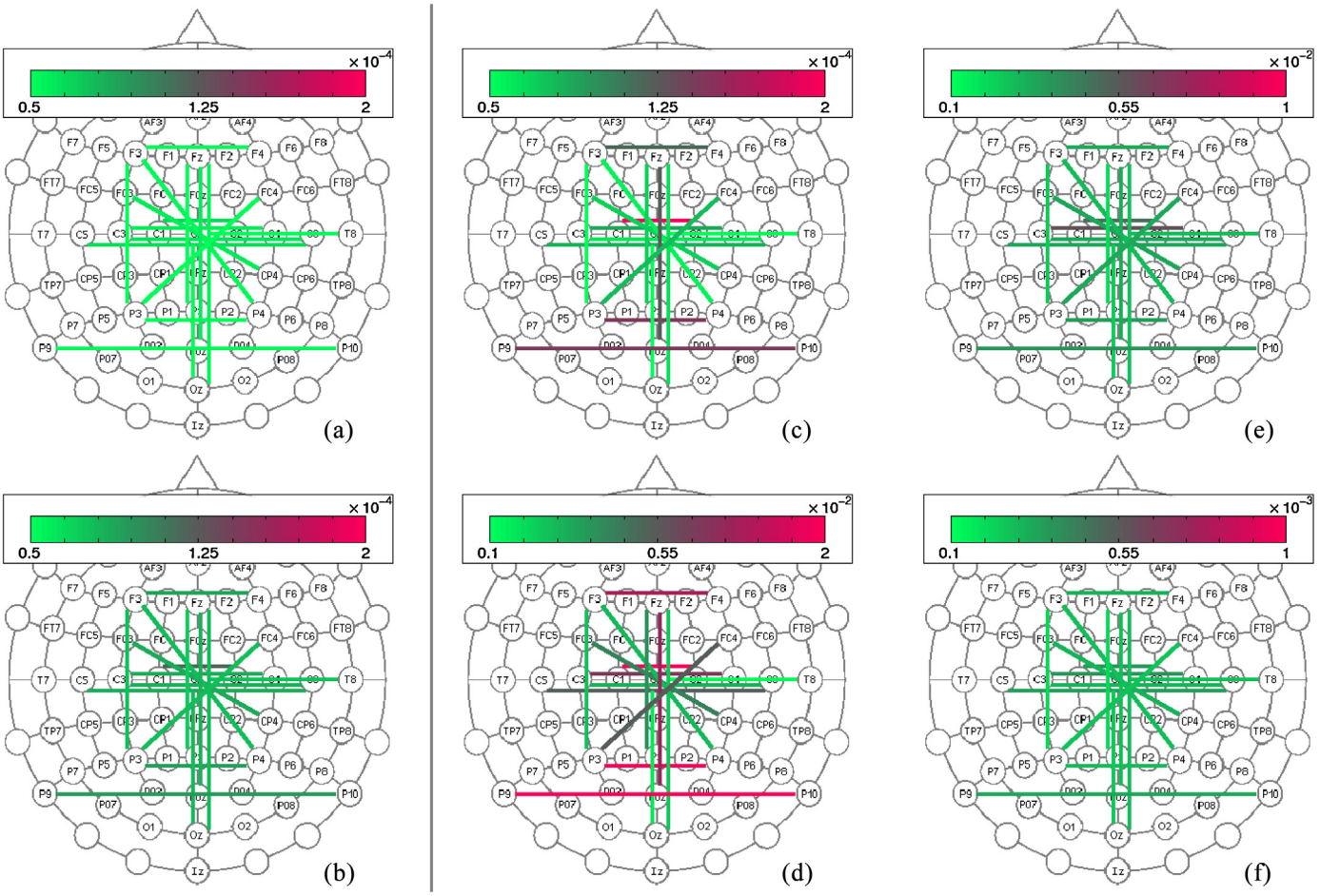

Fig. 4. CVB for the *Partially Isotropic* head model: (a) scalp conductivity and (b) skull conductivity; and for the *Anisotropic* head model: (c) tangential scalp conductivity, (e) radial scalp conductivity, (d) tangential skull conductivity, and (f) radial skull conductivity. The color of each line indicates the CVB value obtained when the current is applied using the electrodes connected by that line. Note that the diagrams have different scales.

electrodes; i.e. the current injection pair. Although the actual value of the CVB depends on the actual configuration of the measuring electrodes, the best pairs usually have a larger distance between injection electrodes, and these are surrounded by a larger number of measuring electrodes. Then, as a general behavior, pairs such as F3–P4, P3–FC4, F3–P3 or Fz–Pz should be preferred. This implies fewer measurements (less measurement time) over these pairs to reach the same relative errors as when using other pairs. A more particular observation is that for the *Isotropic* model, fronto-occipital pairs perform better than left-to-right pairs, as can be seen in Fig. 3. This could be because of the longer path the current must traverse in fronto-occipital pairs, or because the distribution of the electrodes is not invariant when rotated 90 degrees. In all diagrams, the CVB values for most pairs are less than 10^{-2}, i.e. a relative error below 1% in the estimated conductivities. Note that from (6), (7), and (10), the CVB values are inversely proportional to the square root of the number S of trials. So, the results can be easily extrapolated to any number of independent measurements.

To analyze the performance of the MLE in the whole proposed skull conductivity range, we show the results for the 'P3–Fc4' pair as we consider it a representative example. The CVB and ECV are displayed for the *Isotropic* and *Partially Isotropic* models as a function of the skull conductivity in Fig. 5a and b, and for the *Anisotropic* model as a function of the skull anisotropy ratio in Fig. 5c. Note that Fig. 5b also shows the CVB for the parameters of the *Isotropic* model, in order to quantify the benefits of knowing *a priori* the brain conductivity.

In the *Isotropic* and *Partially Isotropic* models, the scalp conductivity estimation presents the lowest relative CRLB. A low CRLB indicates high sensitivity, which means that the scalp is the most influential tissue for the EIT method, in agreement with [4]. However, Fig. 5a and b demonstrates that for high skull conductivities, the influence of the skull and brain increases. The results shown in Fig. 5a, b, and c show that, under the proposed conditions, all the parameters of any of the head models can be estimated using EIT with good quality, i.e. with a very low relative error. This holds for the whole studied range of skull conductivity values and anisotropic conductivity ratios.

In the case of the anisotropic model (Figs. 4(c–f) and 5c), the tangential scalp conductivity and the radial skull conductivity present a lower CVB compared to the radial scalp and tangential skull conductivities. This is because the measured electric potential is more sensitive to the tangential scalp and radial skull conductivities. The lines in Fig. 2 indicate that the current flow is mostly tangential in the scalp and radial in the skull. The zoomed region at the right of the figure provides a closer look at this effect, which is a consequence of the relatively low conductivity of the skull compared to the conductivity of the scalp. However, it is empirically observed in EEG that the parameters with higher relative error (radial scalp and tangential skull conductivities) are those that have a lower influence on EEG source localization.

In Fig. 5b we can observe that the *a priori* knowledge of the brain conductivity map obtained from DTI leads to a three-fold reduction in the relative error of the scalp conductivity estimation and an ~40% reduction of the relative error of the skull conductivity estimation. These results can also be read as a reduction of the total amount of measurements to be made. For example, the *Partially Isotropic* head model would require approximately 10 times less measurements than the *Isotropic* model to obtain a similar relative error for the estimation of the scalp conductivity and half of the measurements for the estimation of the skull conductivity.

When comparing the MLE with the CRLB, note that in Fig. 5a, b and c the CVE value was obtained by computing the standard deviation of only 20 trials, thus these results are rather noisy. However, even with this low number of trials it is evident that the

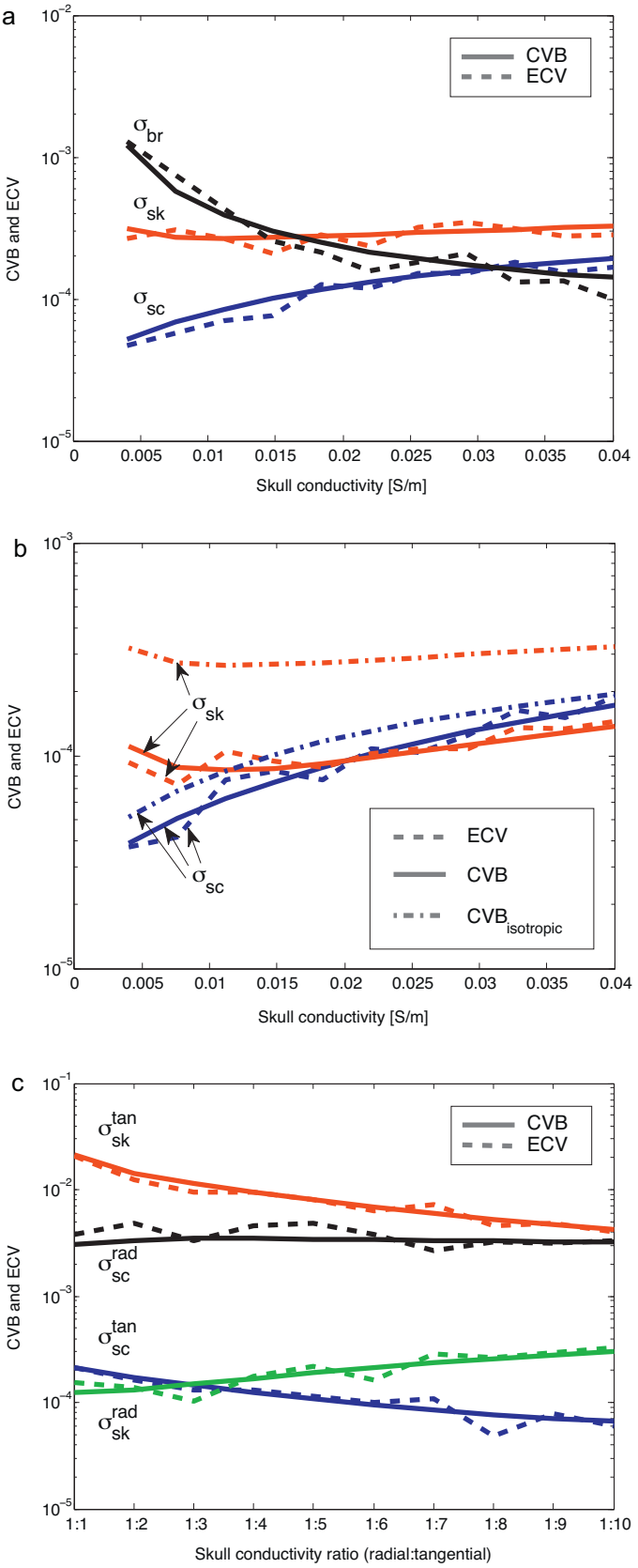

Fig. 5. CVB and ECV as a function of the skull conductivity for the 'P3–Fc4' current injection pair for the (a) *Isotropic*, (b) *Partially Isotropic*, and (c) *Anisotropic* head models. In (b), the CVB for the *Isotropic* model is also displayed.

MLE performs very well for $S = 50$ independent measurements. This behavior was observed in all the pairs under study.

4. Conclusions

The results of this work strengthen the idea of using EIT as a routine together with EEG in all cases where EEG source localization is going to be studied. Also functional EIT and Magnetoencephalography may take advantage of using this combination of EIT and MR imaging to obtain improved impedance models of the head. We also showed that the MLE might be used to estimate the conductivities with a practical number of independent measurements.

As the skull conductivity value, or values assigned to homogeneous or inhomogeneous models remain undefined, EIT appears as a low cost and easy to implement method to obtain these parameters for each particular subject. The combination with DTI not only improves the performance of EIT, but also completes the conductivity model of the head providing the conductivity of the skull, which cannot be obtained from DTI. In functional EIT the brain function is studied by detecting impedance changes due to increased oxygen consumption in active neurons [31]. In this case the frequency of the injected current can be arbitrarily chosen and for high frequencies the characterization of the tissues could require more parameters, such as the electrical permittivity. EIT can also be applied to head models that require the estimation of a larger number of parameters, such as models with more layers.

The use of better skull models, e.g. including its sutures or local variations, is planned as future work. In the case of local variations the use of several electrode pairs would be necessary and the use of the CRLB to choose the most convenient pairs may lead to important savings in measurement time.

Acknowledgements

This work was supported by ANPCyT PICT 2011-11-0909, UNLP 11-I-166, CONICET, and CIC-pBA.

Appendix A. FEM and linear equations

In this Appendix, we describe the FEM method and the derivation of (3), (4) and (5).

The weighted residual method modifies the volume condition in Eq. (1) by requiring

$$\int_{\Omega} \omega \vec{\nabla} \cdot \left(\boldsymbol{\sigma}\left(\vec{x}\right) \vec{\nabla} \boldsymbol{\Phi}\left(\vec{x}\right) \right) d\Omega = 0, \tag{13}$$

where ω is a weight function, $\boldsymbol{\Phi}$ represents the unknown potential, $\boldsymbol{\sigma}(\vec{x})$ represents the 3×3 conductivity tensor at the point $\vec{x}$ and Ω is the head volume. Applying properties of the gradient and the divergence, (13) can be expressed as

$$\int_{\Omega} \vec{\nabla} \cdot (\omega \boldsymbol{\sigma} \vec{\nabla} \boldsymbol{\Phi}) d\Omega - \int_{\Omega} (\vec{\nabla}\omega) \boldsymbol{\sigma} (\vec{\nabla} \boldsymbol{\Phi}) d\Omega = 0, \tag{14}$$

which is known as the weak formulation. Then, applying the Green's Theorem to the first term, we obtain

$$\int_{\Omega} (\vec{\nabla}\omega) \boldsymbol{\sigma} (\vec{\nabla} \boldsymbol{\Phi}) d\Omega = \int_{\delta\Omega} \omega \underbrace{\boldsymbol{\sigma} \vec{\nabla} \boldsymbol{\Phi} \cdot \hat{n}}_{\text{current density } j} \; d(\delta\Omega), \tag{15}$$

where $\hat{n}$ is the normal unit vector to the surface element $d(\delta\Omega)$. Using Galerkin's formulation with linear functions, the condition of Eq. (13) is required for all functions ω of an appropriate set of functions that form a base of the solution space. For each tetrahedron, we adopt four functions ω_i frequently used in FEM, that are equal to 1 at a node of the tetrahedron and decrease linearly to zero at the opposite face. The volume Ω is tessellated into tetrahedrons and the potential $\boldsymbol{\Phi}$ is approximated as a linear combination of the weight functions ω. The integrals $\int_{\Omega} (\vec{\nabla}\omega_i) \boldsymbol{\sigma} (\vec{\nabla}\omega_j) d\Omega$ are solved for each element and for each combination of i and j, which results in a 4×4 element matrix K_e per element. The assembly of all element matrices forms the $n \times n$ system *stiffness matrix* K, where n is the total number of nodes [32]. The left side of Eq. (15) can be expressed as KU, where U is the unknown $n \times 1$ vector of electric potential at the nodes.

During the tessellation process, we make sure that the points corresponding to the electrode positions were vertices of tetrahedrons. Since $\omega = 1$ at the nodes, including the current source and sink points ($\vec{x}_+$ and $\vec{x}_-$), the surface integral from Eq. (15) can be expressed as

$$\int_{\delta\Omega} \omega j(\vec{x}) d(\delta\Omega) = \begin{cases} +I & \text{if } \vec{x} = \vec{x}_+ \\ -I & \text{if } \vec{x} = \vec{x}_- \\ 0 & \text{elsewhere} \end{cases}, \tag{16}$$

where I is the intensity of the electric current. The resulting FEM linear system of equations is

$$KU = F, \tag{17}$$

where the independent vector F is an all zero vector except for $+I$ and $-I$ at the injection node positions.

In linear FEM, the element matrix can be expressed as

$$K_e = \frac{B^T \boldsymbol{\sigma} B}{36V}, \tag{18}$$

where B is a 3×4 transformation matrix that depends on the position of the vertices of a particular tetrahedron of volume V. In the isotropic case, the conductivity tensor is

$$\boldsymbol{\sigma} = \sigma I_3, \tag{19}$$

where I_3 is the 3×3 identity matrix. The conductivity tensor is different in the anisotropic case. It is desirable to express it as

$$\boldsymbol{\sigma} = C \begin{pmatrix} \sigma^t & 0 & 0 \\ 0 & \sigma^t & 0 \\ 0 & 0 & \sigma^r \end{pmatrix} C^{-1}, \tag{20}$$

where C is the change of basis matrix from the canonic base to a tangential/radial one. To define the radial direction, for each tetrahedron the closest triangle on the surface was determined by a projection. As the parameters of the model are the tangential and radial conductivities, the element matrix can be expressed as a function of two new matrices K_e^t and K_e^r:

$$K_e = \frac{1}{36V} B^T C \begin{pmatrix} \sigma^t & 0 & 0 \\ 0 & \sigma^t & 0 \\ 0 & 0 & \sigma^r \end{pmatrix} C^{-1} B = \frac{B^T C}{36V} \left(\sigma^t \begin{pmatrix} 1 & 0 & 0 \\ 0 & 1 & 0 \\ 0 & 0 & 0 \end{pmatrix} + \sigma^r \begin{pmatrix} 0 & 0 & 0 \\ 0 & 0 & 0 \\ 0 & 0 & 1 \end{pmatrix} \right) C^{-1} B = \sigma^t K_e^t + \sigma^r K_e^r. \tag{21}$$

With this procedure, the tangential and radial components of the element matrix can be assembled separately resulting in a system *stiffness matrix* K for each orientation.

References

[1] S. Rush, D. Driscoll, Current distribution in the brain from surface electrodes, Anesth. Analg. 47 (1968) 717–723.

[2] T. Oostendorp, J. Delbeke, D. Stegeman, The conductivity of the human skull: results of in vivo and in vitro measurements, IEEE Trans. Biomed. Eng. 47 (2000) 1487–1492.
[3] R. Sadleir, A. Argibay, Modeling skull electrical properties, Ann. Biomed. Eng. 35 (2007) 1699–1712.
[4] L. Horesh, Some Novel Approaches in Modelling and Image Reconstruction for Multi-Frequency Electrical Impedance Tomography of the Human Brain, Ph.D. thesis, University College London, 2006.
[5] C. Tang, F. You, G. Cheng, D. Gao, F. Fu, G. Yang, X. Dong, Correlation between structure and resistivity variations of the live human skull, IEEE Trans. Biomed. Eng. 55 (2008) 2286–2292.
[6] G. Huiskamp, M. Vroeijenstijn, R. Van Dijk, G. Wieneke, A.C. Van Huffelen, The need for correct realistic geometry in the inverse EEG problem, IEEE Trans. Biomed. Eng. 46 (1999) 1281–1287.
[7] B. Vanrumste, G. Van Hoey, R. Van de Walle, M. D'Hav, I. Lemahieu, P. Boon, Dipole location errors in electroencephalogram source analysis due to volume conductor model errors, Med. Biol. Eng. Comput. 38 (2000) 528–534.
[8] J.-F.P. Abascal, S.R. Arridge, D. Atkinson, R. Horesh, L. Fabrizi, M.D. Lucia, L. Horesh, R.H. Bayford, D.S. Holder, Use of anisotropic modelling in electrical impedance tomography; description of method and preliminary assessment of utility in imaging brain function in the adult human head, NeuroImage 43 (2008) 258–268.
[9] C. Wolters, A. Anwander, X. Tricoche, D. Weinstein, M. Koch, R. MacLeod, Influence of tissue conductivity anisotropy on EEG/MEG field and return current computation in a realistic head model: a simulation and visualization study using high-resolution finite element modeling, NeuroImage 30 (2006) 813–826.
[10] R. Bayford, Bioimpedance tomography (electrical impedance tomography), Annu. Rev. Biomed. Eng. 8 (2006) 63–91.
[11] S. Gonçalves, J.C. de Munck, R.M. Heethaar, F.H.L. da Silva, B.W. van Dijk, The application of electrical impedance tomography to reduce systematic errors in the EEG inverse problem – a simulation study, Physiol. Meas. 21 (2000) 379–393.
[12] T. Ferree, K.J. Eriksen, D. Tucker, Regional head tissue conductivity estimation for improved EEG analysis, IEEE Trans. Biomed. Eng. 47 (2000) 1584–1592.
[13] M. Dannhauer, B. Lanfer, C.H. Wolters, T.R. Knösche, Modeling of the human skull in EEG source analysis., Hum. Brain Mapp. 32 (2011) 1383–1399.
[14] C.H. Wolters, Influence of tissue conductivity inhomogeneity and anisotropy on EEG/MEG based source localization in the human brain, Ph.D. thesis, Max Planck Institute of Cognitive Neuroscience Leipzig, 2003.
[15] S. Gonçalves, J. de Munck, J. Verbunt, F. Bijma, R. Heethaar, F.L. da Silva, In vivo measurement of the brain and skul resistivities using an EIT-based method and realistic models for the head, IEEE Trans. Biomed. Eng. 50 (2003) 754–767.
[16] R. Hoekema, G. Wieneke, F. Leijten, C. van Veelen, P. van Rijen, G. Huiskamp, J. Ansems, A. van Huffelen, Measurement of the conductivity of skull, temporarily removed during epilepsy surgery, Brain Topogr. 16 (2003) 29–38.
[17] D. Güllmar, J. Haueisen, J.R. Reichenbach, Influence of anisotropic electrical conductivity in white matter tissue on the EEG/MEG forward and inverse solution. a high resolution whole head simulation study, NeuroImage 51 (2010) 145–163.
[18] D. Tuch, V. Wedeen, A. Dale, J. George, J. Belliveau, Conductivity tensor mapping of the human brain using diffusion tensor MRI, Proc. Natl. Acad. Sci. U.S.A. 98 (2001) 11697–11701.
[19] S. Mori, K. Oishi, H. Jiang, L. Jiang, X. Li, K. Akhter, K. Hua, A.V. Faria, A. Mahmood, R. Woods, A.W. Toga, G.B. Pike, P.R. Neto, A. Evans, J. Zhang, H. Huang, M.I. Miller, P. van Zijl, J. Mazziotta, Stereotaxic white matter atlas based on diffusion tensor imaging in an ICBM template, NeuroImage 40 (2008) 570–582.
[20] M. Fernández-Corazza, N. von Ellenrieder, C.H. Muravchik, Estimation of electrical conductivity of a layered spherical head model using electrical impedance tomography, J. Phys. Conf. Ser. 332 (2011) 012022.
[21] W. Lionheart, N. Polydordes, A. Borsic, in: D.S. Holder (Ed.), The Reconstruction Problem, Part 1 of Electrical Impedance Tomography: Methods, History and Applications, Inst. Phys., 2004, pp. 3–64.
[22] Z. Xu, W. He, C. He, Z. Zhang, Z. Liu, The analytical solution of EIT forward problem based on a multilayer spherical model, in: World Automation Congress, Hawaii, 2008, pp. 1–5.
[23] J.-F.P.J. Abascal, S.R. Arridge, W.R.B. Lionheart, R.H. Bayford, D.S. Holder, Validation of a finite-element solution for electrical impedance tomography in an anisotropic medium, Physiol. Meas. 28 (2007) S129–S140.
[24] J.O. Ollikainen, M. Vauhkonen, P.A. Karjalainen, J.P. Kaipio, Effects of electrode properties on EEG measurements and a related inverse problem, Med. Eng. Phys. 22 (2000) 535–545.
[25] IEC60601, Medical Electrical Equipment. Part 1: General Requirements for Basic Safety and Essential Performance, ed 3.0, International Electrotechnical Commission, Geneva, 2005.
[26] O. Gilad, L. Horesh, D. Holder, Design of electrodes and current limits for low frequency electrical impedance tomography of the brain, Med. Biol. Eng. Comput. 45 (2007) 621–633.
[27] J. Mazziotta, A. Toga, A. Evans, P. Fox, J. Lancaster, K. Zilles, R. Woods, T. Paus, G. Simpson, B. Pike, C. Holmes, L. Collins, P. Thompson, D. MacDonald, M. Iacoboni, T. Schormann, K. Amunts, N. Palomero-Gallagher, S. Geyer, L. Parsons, K. Narr, N. Kabani, G.L. Goualher, D. Boomsma, T. Cannon, R. Kawashima, B. Mazoyer, A probabilistic atlas and reference system for the human brain: International Consortium for Brain Mapping (ICBM), Philos. Trans. R. Soc. Lond. B: Biol. Sci. 356 (2001) 1293–1322.
[28] H. van der Vorst, BI-CGSTAB: a fast and smoothly converging variant of BI-CG for the solution of nonsymmetric linear systems, SIAM J. Sci. Stat. Comput. 13 (1992) 631–644.
[29] M. Fernández-Corazza, L. Beltrachini, N. von Ellenrieder, C.H. Muravchik, Waveform selection for electrical impedance tomography, IEEE Lat. Am. Trans. 11 (2013) 402–407.
[30] S.M. Kay, Fundamentals of Statistical Signal Processing: Estimation Theory, Prentice-Hall, Inc., Upper Saddle River, NJ, USA, 1993.
[31] D. Holder, Electrical impedance tomography of brain function, in: World Automation Congress, Hawaii, 2008.
[32] Y.W. Kwon, H. Bang, Finite Element Method Using MATLAB, 1st edition, CRC Press, Inc., Boca Raton, FL, USA, 1996.